Heliyon 6 (2020) e04199

Contents lists available at ScienceDirect

Heliyon

journal homepage: www.cell.com/heliyon

Review article

Exploring the nature of the interactions between the molecules of the sodium dodecyl sulfate and water in crystal phases and in the water/vacuum interface

Yosslen Aray [a], José G. Parra [b], Ricardo Paredes [c], Luis Javier Álvarez [d], Antonio Diaz-Barrios [e,*]

[a] Universidad de Ciencias Aplicadas y Ambientales, Facultad de Ciencias, Campus Universitario Norte, Calle 222 No 55-37, Bogotá, Colombia
[b] Universidad de Carabobo, Facultad Experimental de Ciencias y Tecnología, FACYT, Dpto. de Química, Lab. de Química Computacional, Bárbula, Venezuela
[c] Departamento de Física y Matemáticas, Universidad Iberoamericana, Prolongación Paseo de la Reforma, 880, Lomas de Santa Fe, C. P. 01219, Ciudad de México, Mexico
[d] Laboratorio de Simulación, Unidad Cuernavaca, Instituto de Matemáticas, Universidad Nacional Autónoma de México, A.P. 273-3 Admon. 3, Cuernavaca, Morelos, 62251, Mexico
[e] Escuela de Ciencias Químicas e Ingeniería, Yachay Tech, Ciudad del Conocimiento de Yachay, Urcuquí, Ecuador

ARTICLE INFO

Keywords:
Theoretical chemistry
Physical chemistry
Crystal phases
Aggregation of the surfactant molecules
Clustering of the surfactant molecules at the water/vacuum interface
Quantum theory of atoms in molecules
Sodium dodecyl sulfonate
Chemistry
Materials chemistry

ABSTRACT

The nature of the interaction between the molecules of the sodium dodecyl sulfate surfactant forming two crystal phases, one anhydrous, $NaC_{12}H_{25}O_4S$ and the other, $NaC_{12}H_{25}O_4S.H_2O$, hydrated with one water molecule for unit cell, has been studied in detail using the quantum theory of atoms in molecules and a localized electron detector function. It was found that for the anhydrous crystal, the head groups of the surfactant molecules are linked into a head-to-head pattern, by a bond path network of Na–O ionic bonds, where each Na^+ atom is attached to four SO_4^- groups. For the hydrated crystal, in addition to these four bonds for Na+, two additional ones appear with the oxygen atoms of the water molecules, forming a bond paths network of ionic Na–O bonds, that link the Na^+ atoms with the SO_4^- groups and the H_2O molecules. Each H_2O molecule is bonded to two SO_4^- groups via hydrogen bonds, while the SO_4^- groups are linked to a maximum of four Na+ atoms. The phenomenon of aggregation of the sodium dodecyl sulfate molecules at the liquid water/vacuum interface was studied using NVT molecular dynamics simulations. We have found that for surfactant aggregates, the Na+ ions are linked to a maximum of three SO_4^- groups and three water molecules that form Na–O bonds. Unlike hydrated crystal, each of the O atoms that make these Na–O bonds is linked to only one Na+ ion. Despite these differences, like the crystal phases, the surfactant molecules tend to form a head-to-head network pattern of ionic Na–O bonds that link their heads. The present results indicate that the clustering of anionic surfactant at the water/vacuum interface is a consequence of the electrostatic alignment of the cationic and anionic groups as occurs in the crystalline phases of sodium dodecyl sulfate.

1. Introduction

Studies on the molecular arrangement of surfactants at the vacuum-water interfaces [1, 2] have found the formation of molecular aggregates of surfactants at the interfacial region when they have relatively high concentrations of surfactants. Recently, molecular dynamic simulations of 8-phenyl hexadecane sulfonate, located at the n-tetradecane/water interface, have reported similar aggregation of surfactants at low concentration [2]. In that work, Paredes et al. concluded that the interface equilibrium time (several microseconds) is orders of magnitude greater than the obtained in other systems simulated. In fact, there was convincing indication that this slow equilibration process is due to surfactant aggregation at the interfacial region [2]. Therefore, the understanding of the nature of the aggregation in this type of molecules is fundamental and would have strong consequences on their simulation times. Specially, in the case of anionic surfactants, it is imperative to understand the influence of the characteristics of the head group on the molecular structure of these surfactants [1, 3]. Sodium Dodecyl Sulfate (SDS) is one of the most relevant anionic surfactants and it is widely used, as a model substance, in experimental studies and theoretical simulations

* Corresponding author.
E-mail address: adiaz@yachaytech.edu.ec (A. Diaz-Barrios).

https://doi.org/10.1016/j.heliyon.2020.e04199
Received 14 October 2018; Received in revised form 26 April 2020; Accepted 8 June 2020

in order to explain different surface and colloidal phenomena [4] Many of these theoretical simulations have used SDS in monolayers, bilayers and micelles, where this surfactant is considered to be an ideal structural model [5, 6, 7, 8, 9, 10, 11, 12]. SDS surfactant have well-defined and characterized four crystal forms [13], an anhydrous form and three hydrates having the composition SDS.nH2O (n = 1/8, 1/2,1), these systems crystallize with lamellar structures that present distinctive polar and nonpolar regions [13, 14, 15, 16, 17]. The SDS crystalline phases offer a unique opportunity to perform a detailed study of the interactions between the individual SDS molecules in the crystals using quantum mechanical calculations.

The Quantum Theory of Atoms in Molecules, QTAIM, in combination with Density Functional Theory, DFT, is a widely used tool to describe the nature of the chemical bonds [18, 19, 20, 21, 22, 23]. With the DFT methods is possible to determine the exact electron density $\rho(\mathbf{r})$, of molecular systems such as crystals, ions and molecules at their ground states. In contrast, the QTAIM tool allows to do a topological analysis of the electron density $\rho(\mathbf{r})$ in order to study the nature of the chemical bonds. In this case, with QTAIM is possible to determine the bond critical points, BCPs, locate the bond path that is formed between atomic nucleus and make a quantification of the bond strength [18, 21, 22, 23].

Recently, a localized-electrons detector (LED) function, which complement the QTAIM analysis has been presented [24, 25]. This function can be determined using the quantum mechanics local momentum representation as function of the electron density $\rho(\mathbf{r})$ [24, 26]. LED function allows to do a representation in three dimensions of the space in where electrons are localized [24, 26]. This LED function can display, in 3D, the various types of bonding interactions present in molecules and crystals, that can be obtained with the topological analysis of the QTAIM: the shared and the closed shell interactions [25, 27]. Generally, LED contour forms are used as detectors of the bonding interactions present and their values are a measure of the electron localization in a given volume [25, 26, 27].

QTAIM has been used to evaluate the crystals packing of organic molecules that have hydrocarbon chains. In fact, Matta et al [28] demonstrated, by means of this theory, the existence of hydrogen-hydrogen interactions between the hydrogen atoms present in hydrocarbon chains, which can lead to a specific crystal packing. Generally, hydrogen-hydrogen interactions between the hydrogen pairs linked to carbon atoms are weak (homopolar interaction type). Matta et al [29] suggested that these interactions fall into the category of van der Waals interactions and this type of interactions occurs in hydrogen atoms linked to carbon atoms in both saturated and unsaturated hydrocarbon compounds.

In the present work, to further understand the nature of the interaction between the SDS surfactant molecules; the two crystal phases of SDS, anhydrous and with n = 1, have been studied in detail using the QTAIM and the LED function. It has been found that for the anhydrous crystal, the headgroups of the SDS molecules are linked in a head-to-head pattern, through a network of Na–O ionic bonds, where each Na atom is bonded to four SO_4^- groups. Each of this SO_4^- group occupies a volume of 66.864 $Å^3$. For the hydrated crystal, the Na atoms are additionally linked to two H_2O molecules by mean of Na–O ionic bonds. Each water molecule is in turn bonded to two SO_4^- groups via hydrogen bonds producing a general volume increase of 11 $Å^3$ on the SO_4^- groups. These results corroborate that as consequence of hydration [13], the head group volume increases, which results in a growth of the polar interface that produces the separation of the hydrocarbon chains. The hydrogen-hydrogen interactions of the pairs of hydrogen linked to carbon atoms of the hydrocarbon chains were not considered in this work. Finally, the phenomenon of the aggregation of the SDS molecule at the liquid water/vacuum interface has been explored using a molecular dynamics simulation. It has been found that, like the crystalline phases, the surfactant molecules tend to form a head-to-head network pattern of ionic Na–O bonds linking their heads. The present results indicate that the clustering of anionic surfactant at the water/vacuum interface is a consequence of the electrostatic alignment of the cationic and anionic groups as it occurs in the crystalline phases of sodium dodecyl sulfate.

2. Quantum theory of atoms in molecules

The quantum theory of atoms in molecules, QTAIM [18, 19, 20, 21, 22, 23, 30], establishes a quantitative relation between the electron density function $\rho(\mathbf{r})$ (irrespective of how it attained, either from experiments or calculations) and the electronic properties of molecules or crystals. One of the main advantageous features of QTAIM is the provision of a rigorous quantum mechanics and topological definition of atoms [18, 19, 30]. In molecules and crystals, the topology of electron density function $\rho(\mathbf{r})$ is determined from the critical points (CPs) and gradient vector field, $\nabla\rho(\mathbf{r})$ [18, 30]. These CPs are defined by the behavior of gradient vector field, $\nabla\rho(\mathbf{r})$ (the collection of gradient paths vanishes) and are classified by the curvatures in the electron density function $\rho(\mathbf{r})$. For this, three eigenvalues λ_i are necessary, which are associated to the Hessian matrix ($H_{ij} = \partial^2(r)/\partial x_i \partial x_j$). Based on these eigenvalues, the CPs in the electron density function $\rho(\mathbf{r})$ are of four types: minima, maxima and two types of saddle point. Here, the maxima (3, −3) CP has eigenvalues λ_1, λ_2 and $\lambda_3 < 0$, the minima (3, +3) CP corresponds to eigenvalues λ_1, λ_2 and $\lambda_3 > 0$. Finally, saddle points (3, +1) CP and (3, −1) CP have eigenvalues $\lambda_1 > 0$, $\lambda_2 > 0$ and $\lambda_3 < 0$; and $\lambda_1 < 0$, $\lambda_2 < 0$ and $\lambda_3 > 0$, respectively. Every CP has a collection of trajectories or gradient paths associated to the electron density function $\rho(\mathbf{r})$. These trajectories have their origin and end at critical points. The (3, -3) CPs correspond to the maxima of the density function $\rho(\mathbf{r})$. In general, these maxima CPs are present at the nuclear positions. Here, each nucleus is an attractor for a collection of gradient paths in the $\nabla\rho(\mathbf{r})$. The region generated by the gradient paths which terminate at a given attractor, defines the basin of the nuclear positions [18]. At the same time, the critical link point, BCP, lies between two adjoining nuclei. This BCP corresponds to a saddle point called (3, -1) CP. This (3, -1) CP is a saddle point of the electron density function $\rho(\mathbf{r})$ that have the maxima in two directions and minimum in the other [18]. This saddle point is a 2D-atractor and 1D-source in the respective directions. Furthermore, the QTAIM analysis generates the interatomic surfaces, IAS, which are defined by the gradient paths involved with the negative eigenvalue of the (3, -1) CP. These IAS divide the molecules in the volume region called atomic basins. The negative eigenvalues (negative curvatures) of density function $\rho(\mathbf{r})$ in a (3, −1) CP, ρ_b, are associated with the perpendicular contraction of electron density function $\rho(\mathbf{r})$, that produces a contraction of charge toward (3, −1) CP [18]. Additionally, there is a unique pair of trajectories involved with the positive eigenvalue of (3, −1) CP that originates at this point and ends at the two nucleus attractors These two gradient routes characterize a line connecting the nuclei, which are called bond paths. Along this bond path, the charge density is a minimum at (3, −1) CP. Therefore, the charge is completely reduced at (3, −1) CP with respect to neighboring nuclei points on the bond path. In addition, the rest of CPs are associated to the geometrical arrangements of bond paths [18], which describe rings and cages elements present in the structure of molecules and crystals. The (3, +1) CP is present in the interior of the ring when the bond paths are linked forming a ring of bonded atoms. Finally, the (3, +3) CPs are called cage critical points. This type of CPs located in the interior of a cage nuclear arrangement. In a (3, +3) CP, the charge density is a local minimum [20, 27] and in crystals, trajectories of $\nabla\rho(\mathbf{r})$ have its origin at such CPs and terminate at nuclei, bond or ring CPs.

3. The localized electrons detector, LED, function

In quantum theory an observable A can be separated into two fundamental terms: a real portion $A'(r)$ (the local value) and an imagi-

nary portion $\tilde{A}(r)$ (the local spread) [24, 26]. The real portion is associated with the classical approximation of the observable A, while the imaginary portion describe the quantum variation of this observable A [24]:

$$A(\mathbf{r}) \equiv A^{'}(\mathbf{r}) + i\tilde{A}(\mathbf{r}) \quad [1]$$

For the momentum operator $\hat{P} = i\hbar\nabla$, the term representing the local momentum $P(r)$ [24] is defined by the Eq. (2):

$$P(r) = P^{'}(r) + i\tilde{P}(r) = P^{'}(r) - i\frac{\hbar}{2}\frac{\nabla(r)}{(r)} \quad [2]$$

Therefore, the term $\tilde{P}$ called quantum variation is proportional to the relation $\nabla\rho(\mathbf{r})/\rho(\mathbf{r})$. The term $\tilde{P}$ is a direct spatial representation of the volume of the orbital-free of localized electron pairs in atoms and molecules [25, 26]. The density of the kinetic energy of the particle is used to determine the localization of the electron pairs in molecular systems, and hence their momentum $\hat{P}$ is an ideal localized electron pair detector [24], which is defined in terms of the electron density and its gradient in Eq. (3), [24, 25, 26].

$$\mathrm{LED} = \tilde{P}[.\nabla(r)/(r)] = \frac{-\hbar}{2}|\nabla\rho(r)/\rho(r)| \quad [3]$$

The values of $\tilde{P}$ represent the regions where electron pairs are spatially localized, producing bonding regions and regions with atomic shells [24, 25]. Furthermore, with the term $\tilde{P}$ is possible to make| a direct spatial representation of bonding interactions in the molecules. The isosurfaces obtained with LED show the same type of symmetries around the BCPs that the given by the Laplacian of $\rho(\mathbf{r})$ [24, 25]. In this sense, LED shows the diverse types of bonding interactions (closed shell and shared interactions) that are obtained with the analysis of the topology of electron density function $\rho(\mathbf{r})$. This LED determines the local amounts of electrons in spatial regions around the $\rho(\mathbf{r})$ critical points [26, 27]. For the (3, -3) CPs that are nuclear attractors (three negative curvatures) of the $\rho(\mathbf{r})$ gradient field, the LED isosurfaces indicate a high local charge concentration of $\rho(\mathbf{r})$ on the inner core shells electrons. In contrast, for the (3, -1) CP that have 2D attractor (two negative curvatures that are perpendicular to the bond of $\nabla\rho(\mathbf{r})$), the LED isosurface represents the local charge concentration in the bonding zones around the BCPs. The spatial forms of LED contours around these critical points are related to the $\rho(\mathbf{r})$ curvatures [24, 25, 26]. Therefore, for a chemical bond of covalent type formed between two atoms, $|\lambda_3| < |\lambda_1| \cong |\lambda_2|$, the LED isosurfaces have a cylindrical spatial form, where the main axis is aligned with the bond path. In contrast, a chemical bond with closed shell, where the ionic contribution is the most important, $|\lambda_3| > |\lambda_1| \geq |\lambda_2|$, the LED isosurfaces are disks shaped perpendicular to the bond paths [24]. In general, the spatial forms of the LED isosurfaces are used to evaluate the type of interaction and their values represent a measure of the electron localization in a spatial region of the molecule [24, 26].

4. Method of calculations

Anhydrous SDS ($Na^{+}.C_{12}H_{25}O_4S$) have a monoclinic crystal structure with space group P21/c [14]. The unit cell dimensions are $a = 38.915$Å; $b = 4.709$Å; $c = 8.198$Å and $\beta = 93.29°$ and the asymmetric unit is formed by a single SDS molecule (See Figure 1a). The crystal packing consists of double layers of molecules (Fig, 1b). On the other hand, $Na^{+}.C_{12}H_{25}O_4S^{-}.H_2O$, is triclinic, space group $P_{\bar{1}}$, $a = 10.423$Å, $b = 5.662$Å, $c = 28.913$Å, $\alpha = 86.70$, $\beta = 93.44$, $\gamma = 89.55°$ [16]. Each asymmetric unit is built with two waters and two sodium dodecyl sulfate (SDS) molecules with different spatial conformations (See Figure 2a). The SDS molecules have a lamellar array with alternately polar and nonpolar regions. The adjacent polar heads of the same monolayer are displaced in a zigzag fashion along an axis forming a rippled structure (See Figure 2b) [16].

The optimization of the geometries that are present in the cell units was carried out with the DFT methods contained in ADF software [31, 32, 33]. For each system the electron density function $\rho(\mathbf{r})$ was determined using the Kohn-Sham method with the gradient-corrected Perdew--Becke-Ernzerhof (PBE) exchange-correlation functional [34]. The ADF software calculates variational self-consistent solutions for the DFT methods using a highly optimized numerical integration scheme for the estimation of matrix elements associated to the Fock operator [31, 32]. The Coulomb potential is determined using the charge density by means of an accurate fitting [31]. In this paper, the triple-zeta plus polarization basis set (TZP) [35] was used in all calculations. These simulations

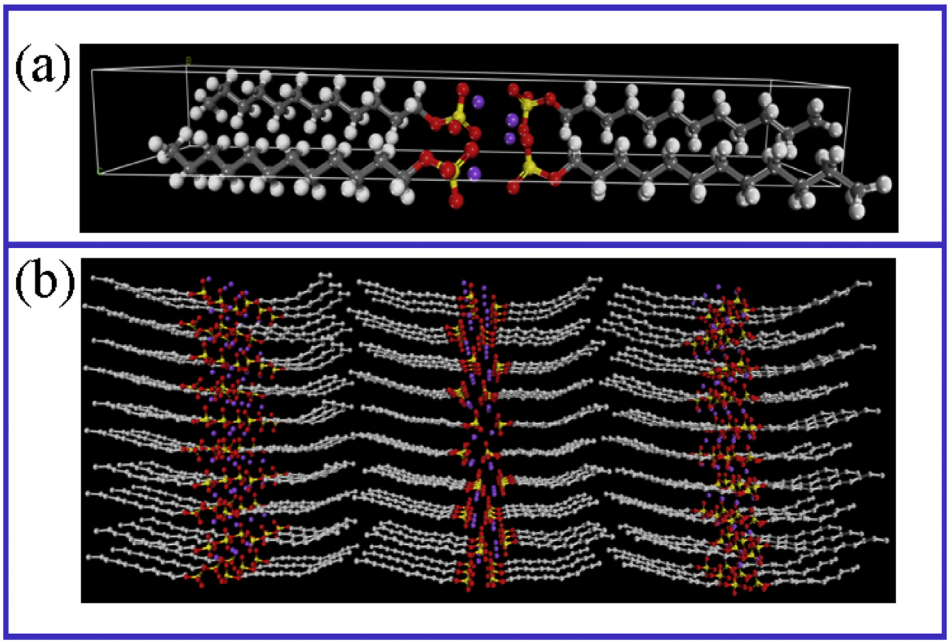

Figure 1. (a) Unit cell of the anhydrous SDS crystal. The white, gray, yellow, red and purple spheres denote the H, C, S, O and Na atoms, respectively. (b) Lamellar structure defined for the anhydrous SDS bulk. The distance tail-tail between the layers measured as the H• • •H distance is 2.016 Å. Three lamellas are shown in the picture.

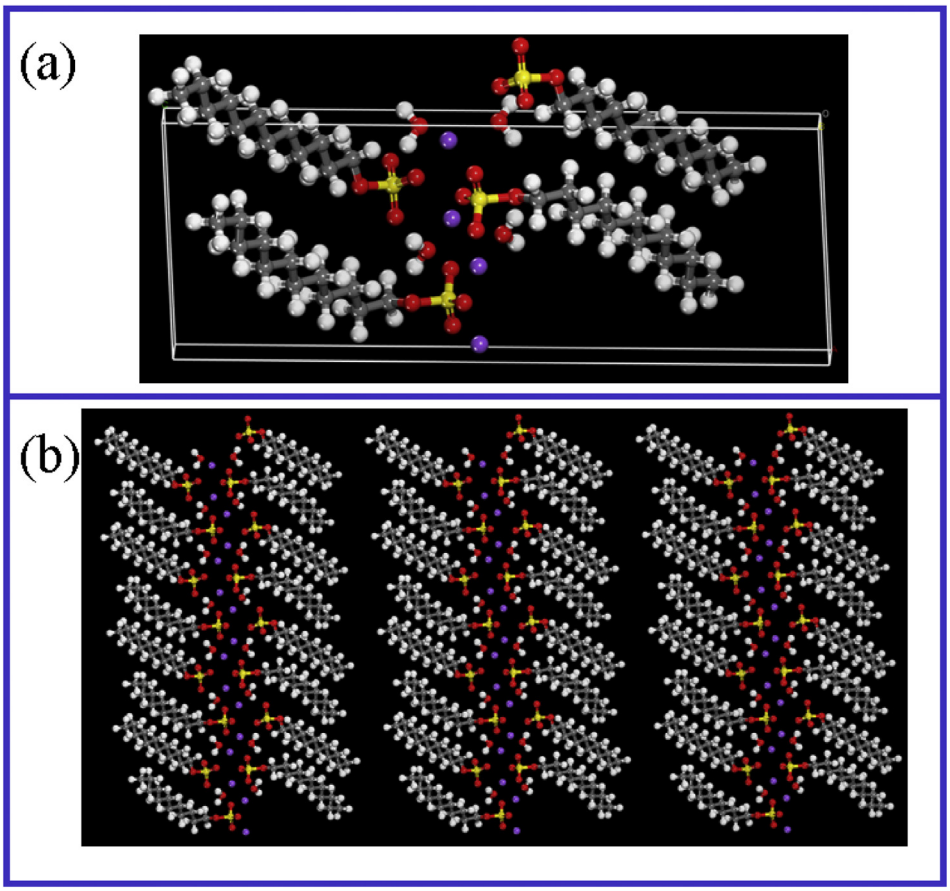

Figure 2. (a) Unit cell of the SDS.1H2O crystal. The white, gray, yellow, red and purple spheres denote the H, C, S, O and Na atoms, respectively. (b) Lamellar structure defined for the hydrated SDS bulk. Three lamellae are shown in the picture. A higher lamellae separation than the case of the anhydrous lamellar structure can be observed (compare with Figure 1b).

determine the molecular electron densities, which are used to carried out the QTAIM analysis and the evaluation of the LED functions of the studied systems [27]. The topology of the electron density function $\rho(\mathbf{r})$ for QTAIM analysis was performed with the method described in the reference 36, using the AIM-UC software [36]. The LED function and the LED isosurfaces were determined with a modified version of the MC33 software, which is described in the references 37 and 38 [37, 38].

5. Results

5.1. SDS molecule

An isolated SDS molecule was built from the Anhydrous SDS unit cell and subsequently optimized using standard ADF methods. For this geometry, all the CPs were located and the topological properties (electron density, ρ_b, the curvatures λ_i and the Laplacian, $\nabla^2\rho_b$) that characterize the head bond critical points are shown in Table 1. The bond paths network (the molecular graph) [18] defining this geometry are shown in Figure 3. Gray, red, yellow and pink denote the C, O, S, and Na atoms, respectively.

The data provided in Table 1, shows that, the C–C BCPs have characteristics associated with covalent type interactions: large ρ_b value, absolute value of λ_1/λ_3higher than 1 and $\nabla^2_{\rho_b} < 0$. All the molecule head bonds show the usual characteristic of polar type interactions, i.e., $\lambda_1/\lambda_3 < 1$. The C–O and S–O bonds show covalent-polar features: $\lambda_1/\lambda_3 < 1$ and $\nabla^2\rho_b < 0$ while the S=O bonds show characteristics of very covalent-polar interactions: large ρ_b value, of $\lambda_1/\lambda_3 < 1$ and $\nabla^2\rho_b >> 0$. The Na–O bonds present close-shell type interactions, with are typical characteristics of ionic bonds such as Na–Cl ($\rho_b = 0.242\ e/\mathring{A}^3$) [20]: very small

Table 1. Bond Critical points properties of ρ(r) for the SDS molecule: electron density, ρ_b, curvatures λ_i *I=1,2* and $j = 3$ are the negative and positive curvatures perpendiculars and parallel to the bonds, respectively; and the Laplacian, $\nabla^2\rho_b$ at the BCP.

Bond	ρ_b $e/\mathring{A}^3$	λ_1	λ_2	λ_3	$\left\|\frac{\lambda_1}{\lambda_3}\right\|$	$\nabla^2\rho_b$ $e/\mathring{A}^5$
C–C	1.658	-11.422	-10.840	9.173	1.245	-13.089
C–O	1.486	-9.159	-9.107	9.493	0.965	-8.773
S–O	1.645	-10.872	-10.047	19.442	0.559	-1.477
S=O	2.076	-12.947	-12.428	36.370	0.356	10.995
S=O	2.155	-14.457	-14.024	44.599	0.324	16.118
S=O	2.132	-14.707	-14.274	41.463	0.355	12.482
Na–O	0.169	-0.747	-0.634	4.816	0.155	3.435
Na–O	0.117	-0.450	-0.193	2.950	0.153	2.307

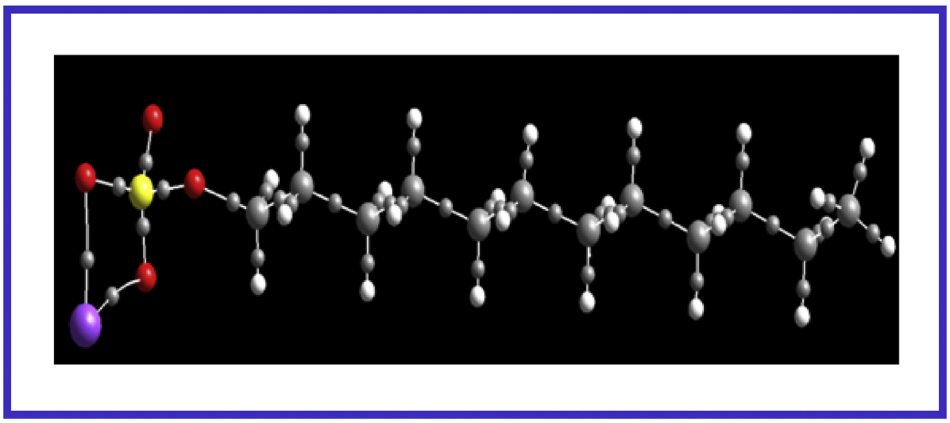

Figure 3. Molecular graph of the SDS isolated molecule. The gray, white, red, yellow and purple spheres denote the C, H, O, S and Na atoms, respectively. Small gray spheres indicate the bond critical points.

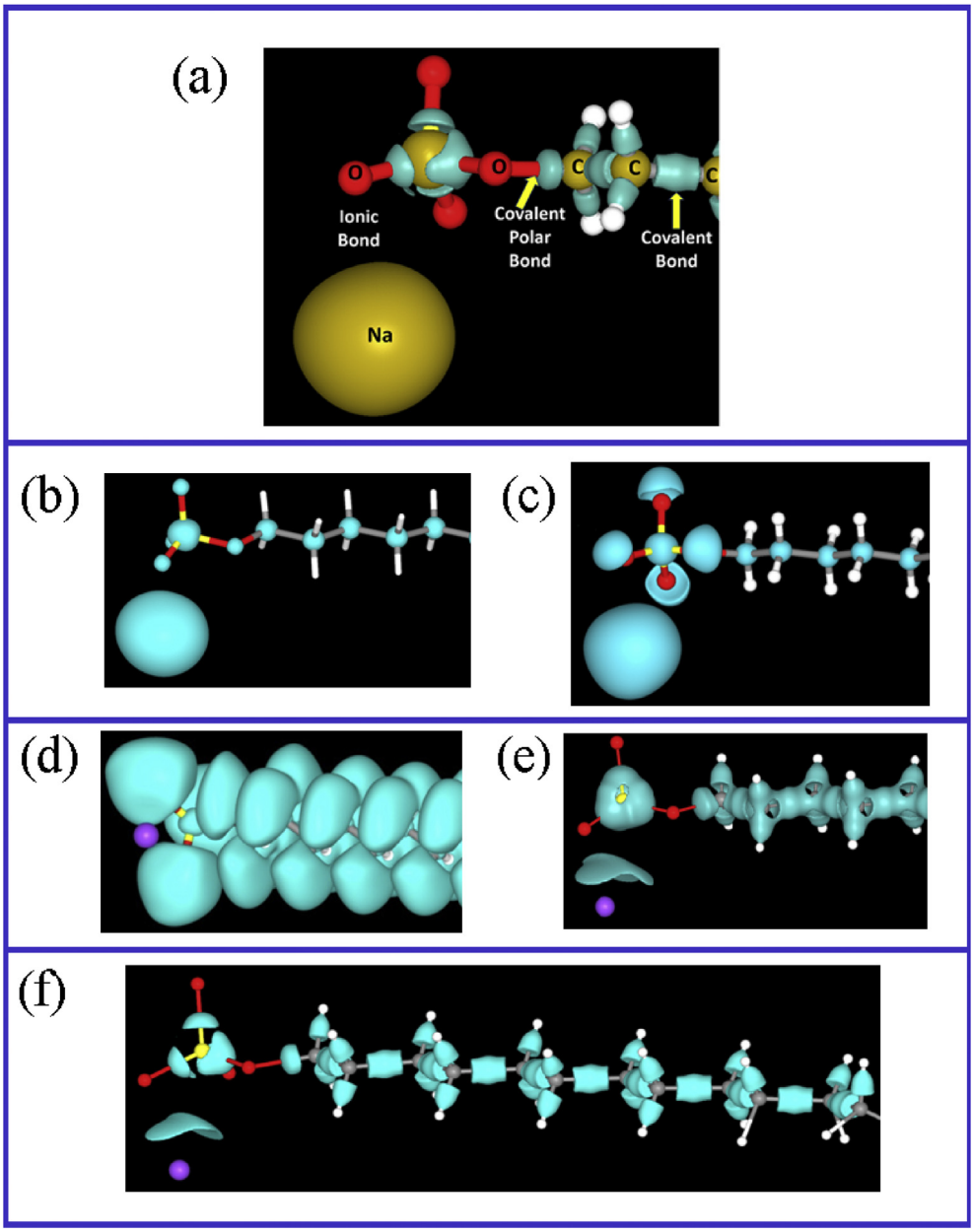

Figure 4. LED isosurfaces for the SDS molecule. (a) LED value of 1.5 au (yellow), containing the core electrons of the C, S and Na atoms while the blue isosurfaces correspond to LED = 0.5 au. These blue areas mainly involve the electron density around the BCPs. The red and white balls represent the O and H atoms, respectively. (b) LED = 1.5 au isosurfaces which encloses the inner core of the heavy atoms. **(c)** LED = 1.2 au isosurfaces showing that for each oxygen atoms a bell-shaped form around the lone pair electrons appeared. (d) LED = 1.0 au and (e) LED = 0.6 au shows the depicted isosurfaces for the C–H bonds. (f). LED = 0.5 isosurfaces let anyone to visualize and explore the nature of all bonds.

Table 2. Bond Critical points properties of $\rho(r)$ for the anhydrous SDS crystal: electron density, ρ_b, curvatures λ_i $I=1,2$ and $j=3$ are the negative and positive curvatures perpendiculars and parallel to the bonds, respectively; and the Laplacian, $\nabla^2\rho_b$ at the BCP.

Bond	ρ_b $e/\text{Å}^3$	λ_1	λ_2	λ_3	$\lvert\frac{\lambda_1}{\lambda_3}\rvert$	$\nabla^2\rho_b$ $e/\text{Å}^5$
C–C	1.683	-13.026	-12.073	8.206	1.587	-16.892
C–O	1.491	-9.336	-8.796	10.929	0.854	-7.203
S–O	1.581	-9.165	-8.610	17.283	0.530	-0.493
S=O	2.008	-13.007	-12.313	41.597	0.313	16.277
S=O	2.051	-14.032	-12.931	49.562	0.283	22.599
S=O	2.086	-14.644	-13.042	51.510	0.284	23.824
Na–O	0.155	-0.647	-0.578	5.100	0.127	3.875
Na–O	0.137	-0.635	-0.588	4.672	0.136	3.448
Na–O	0.188	-0.997	-0.943	6.591	0.151	4.650
Na–O	0.086	-0.339	-0.170	2.617	0.130	2.108

$\rho_b$value and the λ_3 curvature dominates ($\lambda_1/\lambda_3 << 1$), consequently $\nabla^2\rho_b > 0$. In general, the λ_1/λ_3value gives the bond nature trends: the ionic character of a bond increases as the λ_1/λ_3value decreases. Thus, the ionic trend for the SDS molecule bonds is C–C (1.245) < C–O (0.965) < S–O (0.559) < S=O (0.324) < Na–O (0.153).

The nature of these bonds can be easily and directly visualized using the LED function [25, 27]. Thus, Figure 4 shows several LED isosurfaces for SDS. Figure 4a shows regions enclosed by yellow spherical isosurfaces with a LED value of 1.5 au and blue zones corresponding to LED = 0.5 au. The yellow zones that contain the core electrons of the C, S, O and Na

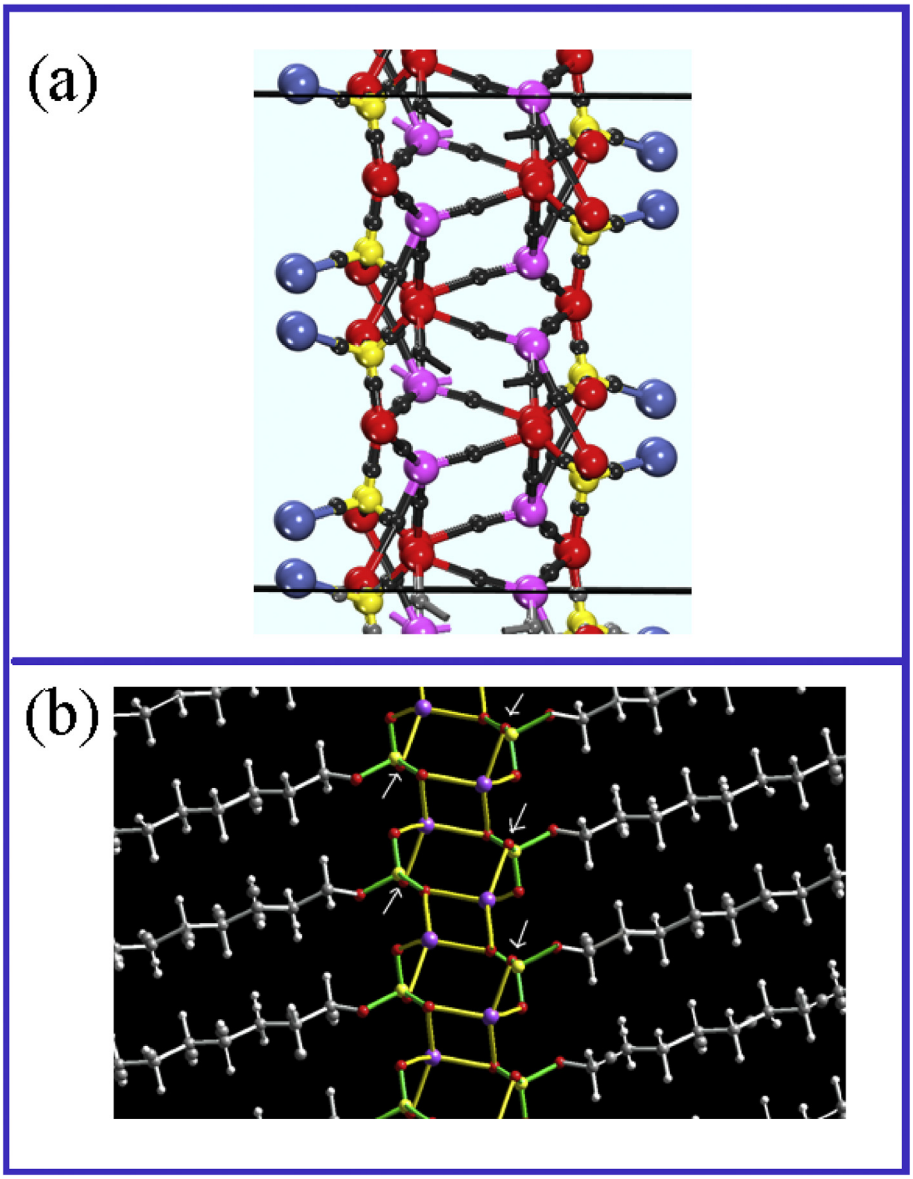

Figure 5. (a) Crystal graph of the heads of the anhydrous SDS system for a unit cell calculated using the AIMUC software [36]. Red, purple and yellow spheres denote the O, Na and S atoms, respectively. Black spheres denote the bond critical points while the dark blue ones highlight the O atoms where the C_{12} tails are linked. (b) Side-view of the anhydrous SDS graph. Green and yellow lines denote the S–O and Na–O bonds, respectively. Gray lines denote the C–C and C–H bonds. White arrows point to O atoms which are bonded to $SO4^-$ groups located behind the picture.

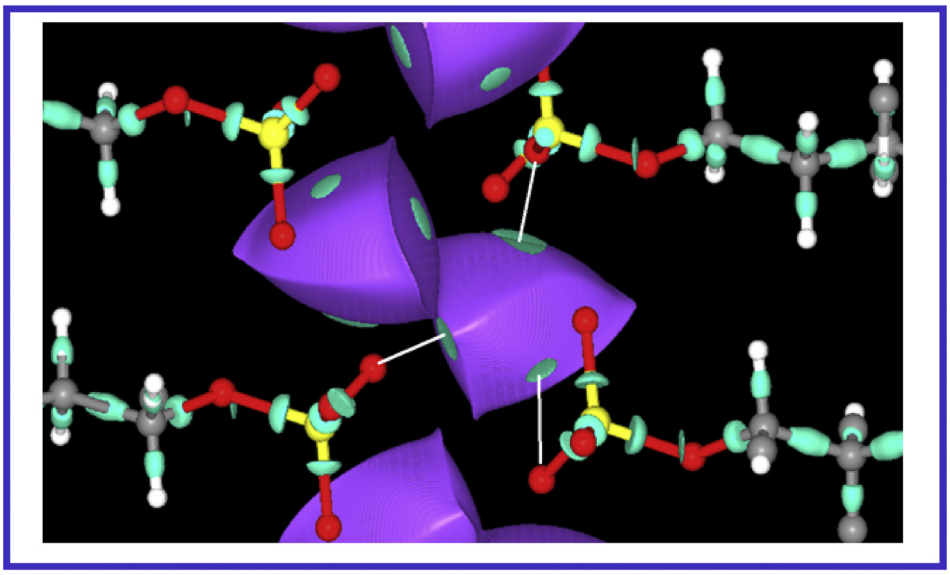

Figure 6. LED = 0.5 au isosurfaces showing the nature of the bonds involve in the SDS anhydrous crystal. In addition, the Na basins (purple zones), i.e., the space occupied by these atoms is also shown. The white lines highlight the Na–O ionic bonds for just one Na atom. The other Na–O ionic bond is behind the plane of the picture.

Table 3. Anhydrous SDS crystal Atomic Charges and volume ($Å^3$). Hydrated $H_{25}C_{12}$–SO_4^- Na.1H_2Ocrystal.

Atom	Group	Atomic Charge	Atomic Volume
Na		+0.895	8.544
Na		+0.889	8.544
Na		+0.889	8.544
Na		+0.895	8.544
O (S=O)		-1.225	16.610
O (S=O)		-1.271	15.933
O (S=O)		-1.262	14.457
O (S–O–C)		-1.009	14.240
S		+3.392	5.6240
	SO_4^-	-1.375	66.864

atoms. The blue areas mainly involve the electron density around the BCPs. The shape of the LED contours around the bond critical points are closely related to the ρ(r) curvatures [25]. For the C–C bonds of the tail, which are typical covalent bond, $|\lambda_3| < |\lambda_1| \cong |\lambda_2|$ and the associated LED isosurface has a perfect cylindrical shape filling the bond zones [25]. For the covalent-polar type bond, C–O, S–O and S=O, $|\lambda_3| > |\lambda_1| \cong |\lambda_2|$ and the LED isosurface corresponds to bent disks perpendicular to the bond paths. These disks are curved towards the least electronegativity atom and fill only part of the bond area. For the Na–O bonds which are pure closed-shell interaction, the LED isosurface around the BCP appears as a very thin region (See Figure 4f) leaving the bond area almost empty.

To better understand the LED function, in Figs. 4b to 4f are shown the different depicted spatial regions of interest for the SDS molecule in the range of 1.5 to 0.5 au. Thus, Figure 4b displays the LED = 1.5 au isosurfaces which enclosee the inner core of the heavy atoms. These zones contain inside all the electron density corresponding the Na, S, C and O core. Spherical contours of LED = 12, 16, 6 and 8 au values (equal to the atomic number and not shown in Figure) denote the limiting regions of the respective atom core. At LED = 1.2 (See Figure 4c) appears, at the non-bonded zones of each oxygen atoms, a bell-shaped form around the lone pair electrons. These O lone-pair zones persist in the range of 1.0 < LED <1.5 au. A curved banana-shape forms that characterize the C–H covalent regions appear at LED = 1.0 au (Figure 4d) and change to a bell-shaped form (Figure 4e) with the top of the bell toward the hydrogen nucleus as the LED value decreases. These forms persist fused to the C atom in the range of 0.6 < LED <1.0 au. At LED = 0.6 au (Figure 4e) the oxygen lone pairs have disappeared and bonded areas around the bonds between the S and O atoms appeared. In addition, the thin disk around

Table 4. Bond Critical points properties of $\rho(r)$ for the $H_{25}C_{12}$–SO_4^- Na.1H_2Ocrystal: electron density, ρ_b, curvatures λ_i *I=1,2* and j = 3; and the Laplacian, $\nabla^2\rho_b$at the BCP.

Bond	ρ_b $e/Å^3$	λ_1	λ_2	λ_3	$\left\|\frac{\lambda_1}{\lambda_3}\right\|$	$\nabla^2\rho_b$ $e/Å^5$
C–O	1.491	-9.343	-8.812	10.928	0.855	-7.227
S–O	1.589	-9.787	-9.042	15.625	0.626	-3.203
S=O	2.144	-15.926	-14.687	48.251	0.330	17.638
S=O	2.235	-18.226	-15.713	57.922	0.315	23.984
S=O	2.287	-19.025	-16.357	60.120	0.316	24.738
Na–O	0.092	-0.391	-0.373	3.028	0.129	2.264
Na–O	0.125	-0.584	-0.505	4.745	0.123	3.655
Na–O	0.154	-0.649	-0.588	5.093	0.127	3.856
Na–O	0.115	-0.500	-0.386	3.703	0.135	2.818
Na–OH_2	0.121	-0.648	-0.500	3.842	0.169	2.649
SO–H_2O	0.320	-2.227	-1.893	7.655	0.291	3.535

the Na–O bond can be equally visualized. Finally, at LED = 0.5 au (Figure 4f) all the areas around the BCPs are depicting. Therefore, these LED = 0.5 isosurfaces provide an appropriate tool to explore the nature of the molecule bonds.

6. Anhydrous SDS crystal

For the optimized cell unit geometry of the anhydrous SDS crystal, all the CPs were also located and the topological properties that characterize the head bond critical points are listed in Table 2. Comparison of Tables 2 and 1 show that, in general, the topological properties and nature of the bonds of the individual molecules, that make up the crystal, are similar to the isolated molecules. Interestingly, for each Na atoms, three of the Na–O bonds exhibit topological values (0.188–0.137 $e/$ Å^3) like the isolated molecules (0.169–0.117 e/Å^3). One of these bonds shows a much lower value (0.086), which is almost half of the other Na–O bonds. Each Na atom has three nearest SO_4^- groups and another one farther away. Overall, the ionic character of the bonds increases as the $\lambda_1/\ \lambda_3$value decreases. The crystal graph (bond paths network) defining the anhydrous SDS geometry is shown in Figure 5. This graph shows that each Na atoms is bonded to four O atoms by BCPs (black spheres in Figure 5a), forming a bond paths network (yellow lines in Figure 5b) of ionic bonds (Na–O) that link the SO_4^- groups (green lines in Figure 5b). Each Na atom is bonded to four O atoms, one by SO_4^- group.

The basin of the Na atoms (purple zones) are shown in Figure 6. The atomic properties in QTAIM are determined by integration of the corresponding property over these basins; where each basin is defined by the set of IASs (Interatomic surfaces) that define the atom [18]. In the present work, the atomic charge and volume for the SDS-head atoms were calculated using the method proposed by Yu et al. [39], implemented and improved in AIMUC-1.5. The obtained results are listed in Table 3 and show that each Na toms has a charge of +0.895e and a volume of 8.544 Å^3; while the SO_4^- shows a charge of -1.375 e and a volume of 66.864 Å^3. Additionally, Figure 6 also shows the isosurfaces depicted by the LED = 0.5 au value. Same to the SDS molecule, for the covalent C–C bonds of the tail, the LED contour has a perfect cylindrical shape filling the bond

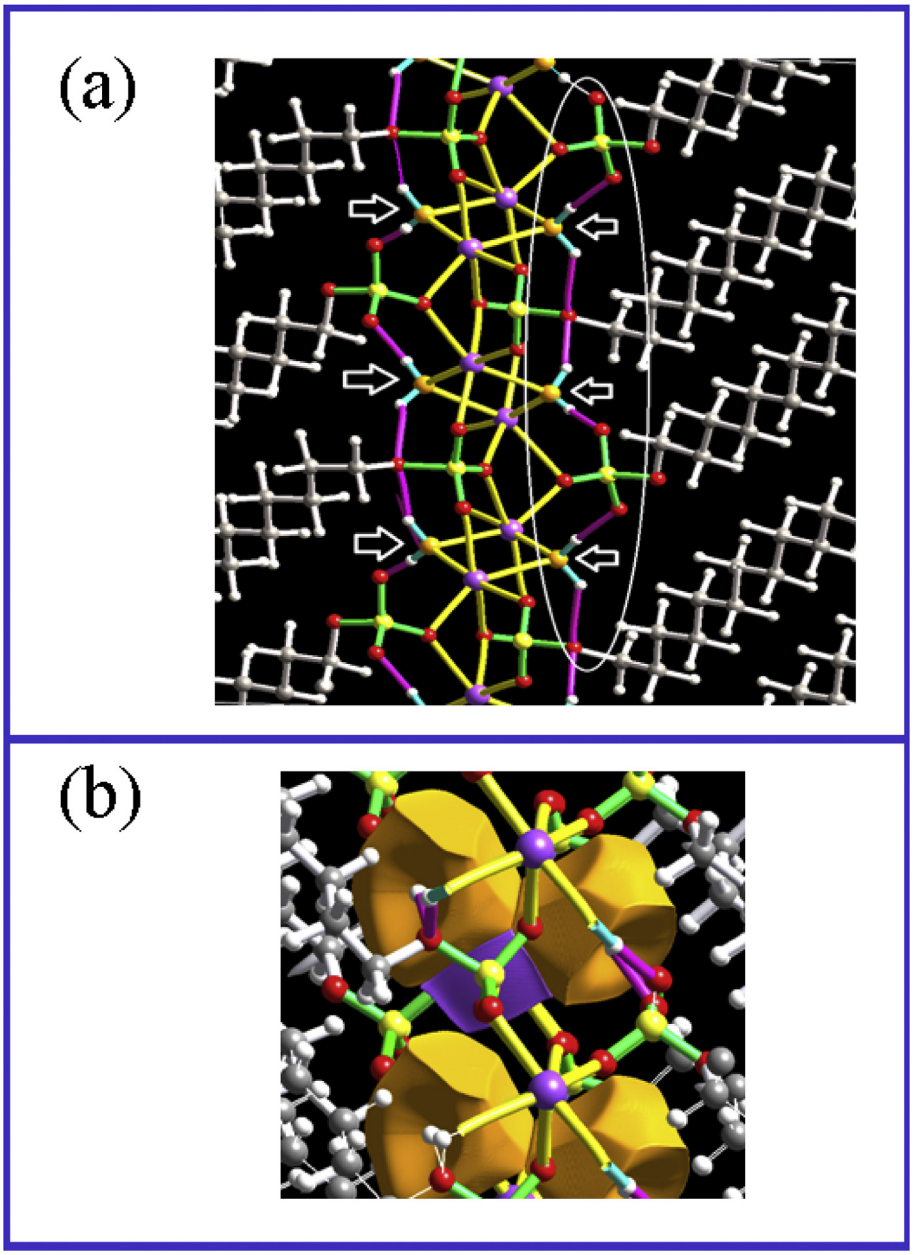

Figure 7. Crystal graph for the unit cell of a layer of the $H_{25}C_{12}$–SO_4^- Na.1H_2O system. (a) Side-view on the unit cell. Gray, white, yellow and pink balls denote the C, H, S, and Na atoms, respectively. Red and orange spheres denote the oxygen atoms of the SO_4^- groups and the water molecules, respectively. Green lines denote the S–O bonds. White arrows highlight the H_2O molecules. Light blue lines denote the H–O water bonds. Pink lines denote the hydrogen bonds between the water molecules and the O atoms of the SO_4^- groups. A white ellipse highlights the fact the water molecules form a kind of casing around the surfactant head. (b) Top-view showing the basin of the Na (pink area) and the O atoms (orange area) of the water molecules surrounding the Na atoms.

Table 5. $H_{25}C_{12}$–SO_4^- Na.1H_2O crystal atomic charges and volume (Å^3).

Atom	Group	Atomic Charge	Atomic Volume
Na		+0.896	8.865
Na		+0.887	8.742
Na		+0.886	8.742
Na		+0.894	8.865
S		+3.640	5.444
O		-1.369	17.950
O		-1.285	18.031
O		-1.298	20.250
O		-1.046	16.223
	SO_4^-	-1.358	77.898
S		+3.532	5.391
O		-1.311	16.609
O		-1.300	17.473
O		-1.283	17.644
O		-1.044	13.461
	SO_4^-		70.578
O		-1.103	20.587
H		+0.593	2.495
H		+0.472	3.918
	H_2O	-0.038	27.000
O		-1.055	19.485
H		+0.501	3.611
H		+0.540	4.485
	H_2O	-0.014	27.581

zones. For the covalent-polar C–O, S–O and S=O bonds, the LED contours corresponds to bent disks, that only fill up part of the bond area; while for the ionic Na–O bonds, the LED isosurfaces around the BCP appear as a very thin region leaving almost empty the bond area.

The topological properties that characterize the head bond critical points of the hydrated crystal with one water molecule by unit cell, are listed in Table 4. In general, the values of $\rho(\mathbf{r})$ at the Na–O bonds, even for the Na-O_{water} bonds, are in a range of 0.096–0.154 au; while the SiO–H_2O hydrogen bonds show a much higher value (0.320 au). This ρ_b and λ_1/λ_3values show that those hydrogen bonds have a higher covalent character than the Na–O bonds. Generally, same to the ionic bonds, the hydrogen bonds exhibit closed shell character [18]. The molecular graph defining this geometry is shown in Figure 7. Gray, white, yellow and purple balls denote the C, H, S, and Na atoms, respectively. The red and orange spheres denote the oxygen atoms of the SO_4^- groups and the water molecules, respectively. This graph shows that each Na atoms is bonded to four O atoms on the SO_4^- groups and two O on the water molecules, forming a bond paths network (yellow lines) of ionic bonds (Na–O) that link the Na atoms with the $H_{25}C_{12}$-SO_4^-chains and the H_2O molecules. The water molecules (light blue lines) are bonded by mean of hydrogen bonds (pink lines) to SO_4^- groups. Table 5 displays the atomic charge and volume of the atoms that make up the SDS head. Comparing with Table 4, it is evident that the water molecules induce a volume increases in the SO_4^- groups from 66.864 Å^3 in the anhydrous crystal to 77.898 Å^3, when just one molecule is inserted in that crystal unit cell. When adding the volume of two water molecules, the resulting SO_4^- .2H_2O groups volume is about 131.898 Å^3. It is clear that H_2O molecules contribute to separate the surfactant layers. Summarizing, the present quantum calculations show that the SDS molecules are linked in a head-to-head pattern by a bond path network of Na–O ionic bonds. For the anhydrous crystal, each Na atom is bonded to four SO_4^- group, occupying a volume of 66.864 Å^3. For the hydrated crystal, each H_2O molecule is bonded to two SO_4^- groups via hydrogen bonds producing a general volume increase of 11 Å^{3}in the SO_4^- groups. These results corroborate that, as consequence of hydration, the head group volume (the sulfate group and associated sodium ions and water) increases, which results in an expansion of the polar interface that produces the separation of the hydrocarbon chains.

7. Molecular dynamics simulations of the SDS molecules adsorption at the water/vacuum interface

Finally, we have explored the phenomenon of aggregation of the SDS molecule at the water/vacuum interface using Molecular-Dynamics, MD, the Compass force field and a NVT (composition, volume and temperature constants) ensemble. The Forcite software [40] with the Compass force field [41] for the MD simulations was used. Initially, an orthorhombic simulation box with dimension of 24 Å × 24 Å × 110 Å containing the water/vacuum interfaces with 900 water molecules was build. The water phase was prepared separately using the Amorphous Builder software [42] to create an initial random and 1.0 g/cm^3 density sample using a suitable Monte Carlo procedure, to achieve a right distribution of the conformational states. After that, this phase was integrated into the simulation box. Then, a monolayer of 14 SDS molecules in a hexagonal arrangement with the hydrophilic head pointing toward water was placed in the simulation box (Figure 8 shows the initial conformation). Two sets, one for the water phase and one for the SDS molecules were defined. The next step was an energy minimization to relax the system. Finally, an NVT simulation of 8 ns at 300K was carried out. The Trajectory analysis gives a final average of the binding energy, BE, between the water phase and the SDS monolayer of -3358.797 Kcal/mol with electrostatic and vdW contributions of -3306.616 and 48.501 kcal/mol, respectively.

Figures 9a and 9b show a snapshot of the final configuration. Figure 9a shows the cross-sectional view perpendicular to the plane of the interface. This picture clearly illustrates the formation of SDS

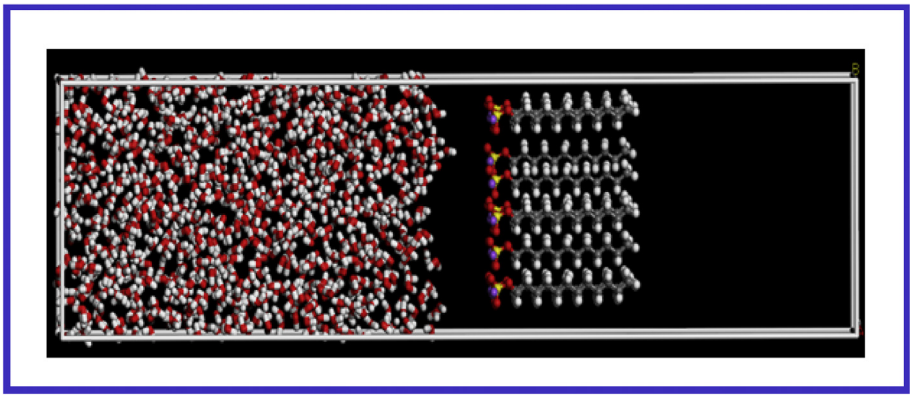

Figure 8. Simulation box showing the initial conformation of the water phase and the SDS monolayer. Red, white, gray, yellow and pink spheres denote the O, H, C, S, and Na atoms, respectively.

aggregates at the water/vacuum interface. Figures 9b and 9d show the top-view for just the SDS-aggregates heads at the monolayer formed at the water/vacuum interface.

Interestingly, these top-view shows that these SDS aggregates tend to form a kind of structures that resemble those of the crystalline states, where the water molecules and, the Na^+ atoms and SO_4^- groups of the SDS heads are electrostatically bonded (See Figure 7). Comparable results, where the formed clusters at the water/vacuum interface tend to be linear, aligning phenyl-SO_3^- groups and Na+ atoms, were reported in ref. 2.

To better understand the nature of this aggregation, Figure 10 shows the bond path network of the hydrated crystal and the last configuration snapshot for the 14 SDS molecules adsorbed at the water/vacuum interface. Figure 10a shows the side-view of the bond paths graph of the surfactant heads of a 2 × 1 unit cell of this crystal. For clarity, the tails are removed and only the bond pattern of the SDS heads is shown. In

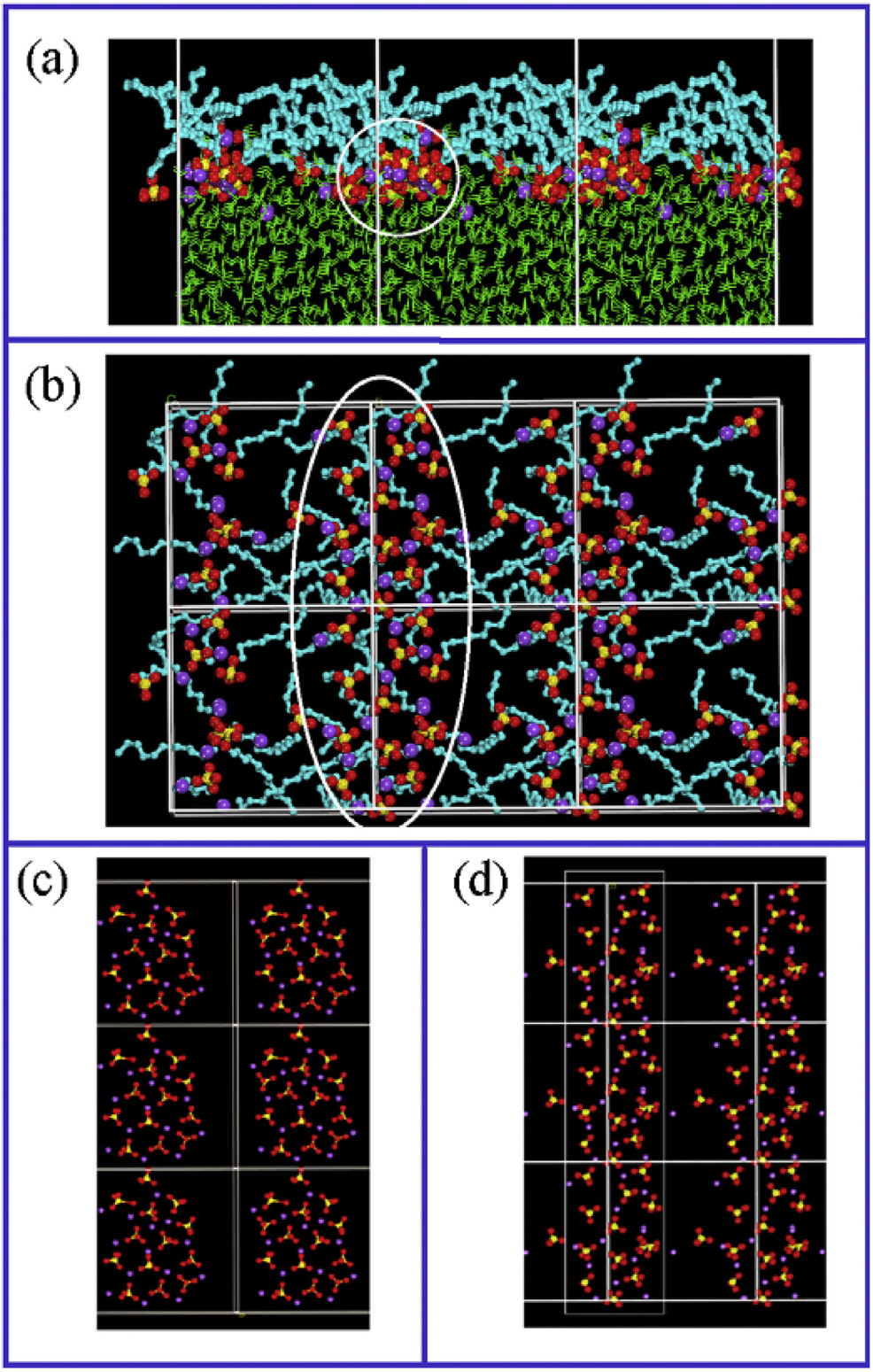

Figure 9. (a) Snapshot of the side-view of the simulation box showing the last configuration of the SDS molecules at the water/vacuum interface. A white circle highpoint just one formed aggregate. (b) Snapshot showing the top-view of the simulation box. A white oval highlights the fact that the SDS heads show the tendency to organize themselves along a line. (c) Top-view of the monolayer formed by 14 SDS molecules heads at the water/vacuum interface at 2 ns and (d) at 8 ns of NVT simulation. For clarity in (c) and (d) the aliphatic chains have been removed. A white square highlights the fact that the Na–SO_4 groups tend to form linear structures.

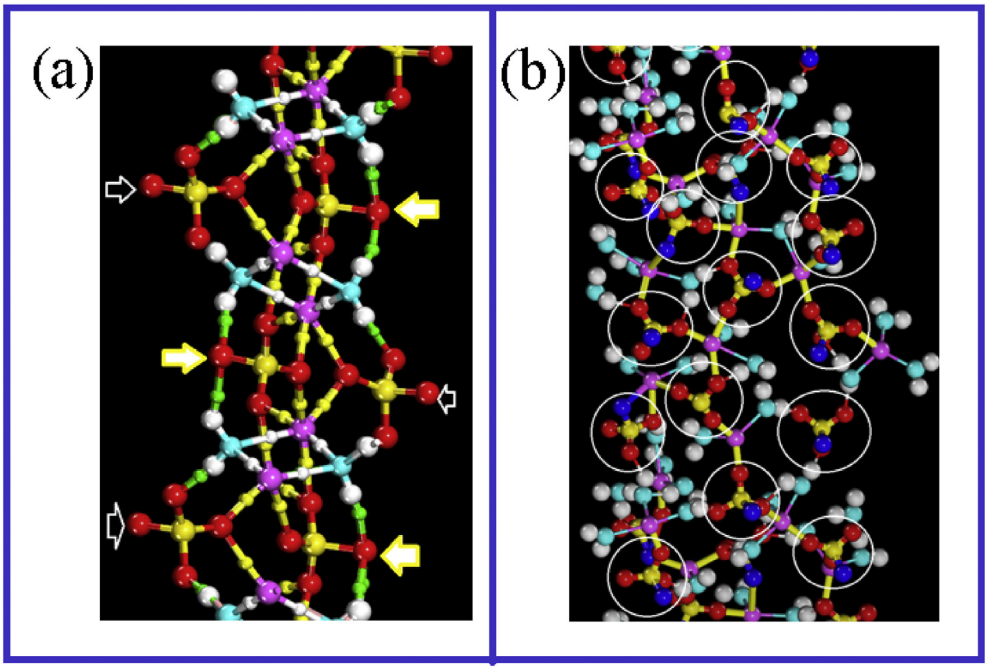

Figure 10. (a) Side-view of a 2 × 1unit cells showing the Crystal graph of the hydrated crystal. The arrows point to the oxygen atoms where the aliphatic chains are bonded. Yellow arrows point to the SO_4 groups linked to four Na^+ ions. For clarity the surfactant hydrophobic tails have been removed. Yellow and white straight lines highlight the Na–OSO_3 and Na–OH_2 bonds, respectively. This graph extends to infinity above and below the picture plane. (b) Bond graph of one of the monolayer aggregates within the white oval of Figure 9b. The gray, white, yellow, red, and purple spheres denote de C, H, S, O and Na toms, respectively. The light blue spheres denote the oxygen atoms of the water molecules and the dark blue spheres denote the O atoms of the $SO4^-$ groups where the hydrophobic tails are linked. In (b) white circles highlight the $SO4^-$ groups bridging the Na atoms.

this graph, each Na+ atom (purple spheres) is bonded to four SO_4^- groups (yellow lines) and two molecules of H_2O (white lines). Note that for one SO_4^- group (top-right of the picture), the O atom (highlighted with a yellow arrow), coordinated to the C_{12} tail, is linked by hydrogen bonds (green lines) to two H_2O molecules, while that each of the other three O atoms, no coordinated to the surfactant tail, is shared with its nearest two Na atoms. This SO_4^- group is linked to four Na+ atoms. For the other SO_4^- group (locate at the left-top of the picture), only one O atom is shared with two Na atoms, while two other O ones are linked by H-bonds to two H_2O molecules. This SO_4^- group is linked to two Na+ atoms. This obtained pattern is repeated along the network of Na–O_4S bonds.

A similar view of the bond pattern for the aggregates highlighted in Figure 9b (inside the white oval) forming the surfactant monolayer at the water/vacuum interface, is shown in Figure 10b. Dark blue spheres denote the O atom of the SO_4^- groups where the surfactant tails are bonded. These hydrocarbon chains are just at the vacuum and above the picture plane. Using the Material Studio software [43], the 14 SDS molecules inside the simulation box were selected and then the water molecules located around the Na atoms (underlined with light blue spheres) in a radio less than 2.3 Å were additionally selected. The electronic density and QTAIM analysis of the final cluster were calculated using the methodology described in the Method of Calculations Section. It can be seen the Na+ ions are linked to a maximum of three SO_4^- groups by mean of ionic Na–O bonds (highlighted with yellow lines) and three water molecules. Contrary to the hydrated crystal, each of the O atoms forming these Na–O bonds is linked just only to one Na+ ion. Despite these differences, like the crystal phases, the surfactant molecules tend to form a head-to-head network pattern of ionic Na–O bonds linking their heads. Therefore, the present results suggest that the clustering of anionic surfactant at the water/vacuum interface is a consequence of the electrostatic aligning of the cationic and anionic groups such as it happens in the crystalline phases of SDS.

8. Summary and conclusions

The nature of the interaction between the SDS surfactant chains of the two crystal phases of SDS, anhydrous: $NaC_{12}H_{25}O_4S$ and hydrated: $NaC_{12}H_{25}O_4S.H_2O$, with one water molecule for unit cell, have been studied in detail using the quantum theory of atoms in molecules and the LED function. It was found that for the anhydrous crystal, the head groups of the SDS molecules are linked into a head-to-head pattern, through a bond path network of Na–O ionic bonds, where each Na^+ atom is bonded to four SO_4^- groups. The nature of the bond between the SDS molecules was analyzed using the LED function. This analysis has shown that for the covalent C–C bonds of the tail, the LED isosurfaces have a perfect cylindrical shape that fills the bond zones. For the covalent-polar C–O, S–O and S=O bonds, the LED surfaces correspond to bent disks that only fill up part of the bond area; while for the ionic Na–O bonds, the LED isosurfaces around the BCP appear as a very thin region that leaves the bond area almost empty. For the hydrated crystal, each Na atoms is bonded to four O atoms and two O on the water molecules, forming a bond paths network of ionic Na–O bonds that link the Na toms with the $H_{25}C_{12}$–SO_4^- molecules and the H_2O molecules. Each H_2O molecule is bonded to two SO_4^- groups through hydrogen bonds producing a general volume increase of 11 $Å^3$ in the SO_4 groups. These results corroborate that, as consequence of hydration, the volume of the head group increases, which results in an expansion of the polar interface that produces the separation of the hydrocarbon chains.

The phenomenon of aggregation of the SDS molecule at the water/vacuum interface was also studied using NVT molecular dynamics simulations. We have found that the clustering of anionic surfactant at the water/vacuum interface is a consequence of the electrostatic alignment of the cationic and anionic groups such as those formed in the SDS crystal phases.

Declarations

Author contribution statement

All authors listed have significantly contributed to the development and the writing of this article.

Funding statement

This research did not receive any specific grant from funding agencies in the public, commercial, or not-for-profit sectors.

Competing interest statement

The authors declare no conflict of interest.

Additional information

No additional information is available for this paper.

References

[1] L. Shi, N.R. Tummala, A. Striolo, C12E6 and SDS surfactants simulated at the vacuum-water interface, Langmuir 26 (2010) 5462–5474.

[2] R. Paredes, A.I. Farinas-Sanchez, B. Medina-Rodriguez, S. Samaniego, Y. Aray, L.J. Alvarez, Dynamics of surfactant clustering at interfaces and its influence on the interfacial tension: atomistic simulation of a sodium hexadecane–benzene sulfonate–tetradecane–water system, Langmuir 34 (2018) 3146–3157.

[3] W.L. Hinze, Organized surfactant assemblies in separation science, in: W.L. Hinze, D. Armstrong (Eds.), Ordered Media in Chemical Separation, ACS Symposium Series: American Chemical Society, Washington, DC, 1987, pp. 2–82. Chapter 1, 342.

[4] (a) K. Kinoshita, E. Parra, D. Needham, Adsorption of ionic surfactants at microscopic air water interfaces using the Micropipette interfacial area-expansion method: measurement of the diffusion coefficient and renormalization of the mean ionic activity for SDS, J. Colloid Interface Sci. 504 (2017) 765–779;
(b) J. Magnus, E. Tyrode, Study of the adsorption of sodium dodecyl sulfate (SDS) at the air/water interface: targeting the sulfate headgroup using vibrational sum frequency spectroscopy, Phys. Chem. Chem. Phys. 7 (2005) 2635–2640.

[5] K. Watanabe, M. Ferrario, M.L. Klein, Molecular dynamics study of a sodium octanoate micelle in aqueous solution, J. Phys. Chem. 92 (1988) 819–821.

[6] Alexander D. Mackerell Jr., Molecular dynamics simulation analysis of a sodium dodecyl sulfate micelle in aqueous solution: decreased fluidity of the micelle hydrocarbon interior, J. Phys. Chem. 99 (7) (1995) 1846–1855.

[7] J. Shelley, M. Shelley, Computer simulation of surfactant solutions, Curr. Opin. Colloid Interface Sci. 5 (2000) 101–110.

[8] C.D. Bruce, M.L. Berkowitz, L. Perera, M.D.E. Forbes, Molecular dynamics simulation of sodium dodecyl sulfate micelle in Water micellar structural characteristics and counterion distribution, J. Phys. Chem. B 106 (2002) 3788–3793.

[9] N. Yoshii, S. Okazaki, A molecular dynamics study of surface structure of spherical SDS micelles, Chem. Phys. Lett. 426 (2006) 66–70.

[10] N. Yoshii, S. Okazaki, A molecular dynamics study of structure and dynamics of surfactant molecules in SDS spherical micelle, Condens. Matter Phys. 10 (2007) 573–578.

[11] M. Sammalkorpi, M. Karttunen, M. Haataja, Structural properties of ionic detergent Aggregates A large-scale molecular dynamics study of sodium dodecyl sulfate, J. Phys. Chem. B 111 (2007) 11722–11733.

[12] M. Sammalkorpi, M. Karttunen, M. Haataja, Ionic surfactant aggregates in saline solutions: sodium dodecyl sulfate (SDS) in the presence of excess sodium chloride (NaCl) or calcium chloride (CaCl2), J. Phys. Chem. B 113 (2009) 5863–5870.

[13] M.D. Ward, M. Horner, J. Structure and order in soft matter: symmetry transcending length scale, CrystEngComm 6 (2004) 401–407.

[14] L.A. Smith, R.B. Hammond, K.J. Roberts, D. Machin, G. McLeod, Determination of the crystal structure of anhydrous sodium dodecyl sulphate using a combination of synchrotron radiation powder diffraction and molecular modelling techniques, J. Mol. Struct. 554 (2000) 173–182 (anhydrous form).

[15] S. Sundell, The crystal structure of sodium dodecylsulfate, Acta Chem. Scand. A31 (1977) 799 (1/2 H2O).

[16] V.M. Coiro, F. Mazza, G. Pochetti, Crystal phases obtained from aqueous solutions of sodium dodecyl sulfate. The structure of a monoclinic phase of sodium dodecyl sulfate hemihydrate, Acta Crystallogr. C42 (1986) 991–995 (1 H2O).

[17] V.M. Coiro, M. Manigrasso, F. Mazza, G. Pochetti, Structure of a triclinic phase of sodium dodecyl sulfate monohydrate. A comparison with other sodium dodecyl sulfate crystal phases, Acta Crystallogr. C43 (1987) 850–854.

[18] R.F.W. Bader, Atoms in Molecules: A Quantum Theory, Clarendon Press, Oxford, 1990.

[19] P.L.A. Popelier, Atoms in Molecules – an Introduction, Pearson Education, Harlow, 2000.

[20] C.F. Matta, R.J. Boyd, An introduction to the quantum theory of atoms in molecules (QTAIM), in: C.F. Matta, R.J. Boyd (Eds.), The Quantum Theory of Atoms in Molecules: from DNA to Solid and Drug Design, 2007, pp. 1–33. Ch. 1.

[21] Y. Aray, J. Rodríguez, D. Vega, Topology of the electron density and cohesive energy of the face-centered cubic transition metals, J. Phys. Chem. B 104 (2000) 4608–4612.

[22] T.Y. Nikolaienko, L.A. Bulavin, D.M. Hovorun, Bridging QTAIM with vibrational spectroscopy: the energy of intramolecular hydrogen bonds in DNA-related biomolecules, Phys. Chem. Chem. Phys. 14 (2012) 7441–7447.

[23] P. Munshi, T.N. Guru Row, Exploring the lower limit in hydrogen bonds: analysis of weak C–H···O and C–H···π interactions in substituted coumarins from charge density analysis, J. Phys. Chem. A 109 (2005) 659–672.

[24] H. Bohorquez, R.J. Boyd, A localized electrons detector for atomic and molecular systems, Theor. Chem. Acc. 127 (2010) 393–400.

[25] H. Bohorquez, C.F. Matta, R.J. Boyd, The localized electrons detector as an ab initio representation of molecular structures, Int. J. Quant. Chem. 110 (2010) 2418.

[26] L.E. Seijas, A. Lunar, L. Rincon, R.J. Almeida, On the electron density localization in HF cyclic clusters, J. Compt. Meth. Sci. Eng. 17 (2017) 5–18.

[27] (a) Y. Aray, R. Paredes, L.J. Álvarez, A. Martiz, On the electron density localization in elemental cubic ceramic and FCC transition metals by means of a localized electrons detector, J. Chem. Phys. 146 (2017) 224504–224508;
(b) Y. Aray, Exploring the electron density localization in single MoS_2 monolayers by means of a localize-electrons detector and the quantum theory of atoms in molecules, AIP Adv. 7 (2017) 115106.

[28] C.F. Matta, J. Hernández-Trujillo, T.H. Tang, R.F. Bader, Hydrogen-hydrogen bonding: a stabilizing interaction in molecules and crystals, Chem. Eur J. 9 (9) (2003) 1940–1951.

[29] J.C. García-Ramos, F. Cortés-Guzmán, C.F. Matta, On the nature of hydrogen-hydrogen bonding, Chapter 16, in: J.J. Novoa (Ed.), Intermolecular Interactions in Molecular Crystals: Fundamentals of Crystal Engineering, Royal Society of Chemistry, London, UK, 2018, pp. 559–594.

[30] R.F.W. Bader, A quantum theory of molecular structure and its applications, Chem. Rev. 91 (1991) 893–928.

[31] S.C.M. ADF2017, Theoretical Chemistry, Vrije Universiteit, Amsterdam, The Netherlands, 2017. http://www.scm.com.

[32] (a) G. te Velde, F.M. Bickelhaupt, E.J. Baerends, C. Fonseca-Guerra, S.J.A. van Gisbergen, J.G. Snijder, T. Ziegler, Chemistry with ADF, J. Comp. Chem. 22 (2001) 931–967;
(b) J.I. Rodriguez, R.F.W. Bader, P.W. Ayers, C. Michel, W. Götz A, C. Boc, A high performance grid-based algorithm for computing QTAIM properties, Chem. Phys. Lett. 472 (2009) 149–152;
(c) J.I. Rodriguez, J. Autschbach, J.F. Castillo-Alvarado, I. María, M. Baltazar-Méndez, Size evolution study of "molecular" and "atom-in-cluster" polarizabilities of medium-size gold clusters, J. Chem. Phys. 135 (2011) 34109;
(d) J.I. Rodriguez, M.I. Baltazar-Méndez, J. Autschbach, F. Castillo-Alvarado, Molecular (global) and atom-in-cluster (local) polarizabilities of medium-size gold nanoclusters: isomer structure effects, Eur. Phys. J. D 67 (2013) 109;
(e) J.I. Rodriguez, An efficient method for computing the QTAIM topology of a scalar field: the electron density case, J. Comput. Chem. 34 (2013) 681–686.

[33] L. Versluis, T. Ziegler, The determination of molecular structures by density functional theory. The evaluation of analytical energy gradients by numerical integration, J. Chem. Phys. 88 (1988) 322–328.

[34] P. Perdew, K. Burke, M. Ernzerhof, Generalized gradient approximation made simple, Phys. Rev. Lett. 77 (1996) 3865.

[35] E. van Lenthe, E.J. Baerends, Optimized Slater-type basis sets for the elements 1–118, J. Compt. Chem. 24 (2003) 1142–1156.

[36] D. Vega, D.J. Almeida, AIM-UC: an application for QTAIM analysis, J. Comput. Methods Sci. Eng. 14 (2014) 131–136. http://alfa.facyt.uc.edu.ve/quimicomp/Vega.

[37] D. Vega, Y. Aray, J. Rodríguez, C library for topological study of the electronic charge density, J. Comput. Chem. 33 (2012) 2526–2531.

[38] Y. Aray, J. Rodríguez, D. Vega, Atoms in Molecules theory for exploring the nature of the active sites on surfaces, in: C.F. Matta, R.J. Boyd (Eds.), The Quantum Theory of Atoms in Molecules: from DNA to Solid and Drug Design, 2007, pp. 231–256.

[39] (a) M. Yu, D.A. Trinkle, Accurate and efficient algorithm for Bader charge integration, J. Chem. Phys. 134 (2011) 64111;
(b) J.S.M. Anderson, P.W. Ayers, J.I.R. Hernandez, How ambiguous is the local kinetic energy? J. Phys. Chem. A 114 (2010) 8884–8895;
(c) L. Cohen, Representable local kinetic energy, J. Chem. Phys. 80 (1984) 4277–4279.

[40] Forcite Is Available as Part of Material Studio, Accelrys Inc, San Diego. USA, 2016.

[41] H. Sun, COMPASS an ab initio force-field optimized for condensed-phase Applications overview with details on alkane and benzene compounds, J. Phys. Chem. B 102 (1998) 7338–7634.

[42] Amorphous Cell Is Available as Part of Material Studio, Accelrys Inc., San Diego. USA, 2016.

[43] Dassault Systèmes Biovia, Materials Studio 8.0, Dassault Systèmes, San Diego, 2014.